Phase space tomography for measuring partially coherent fields of light sources

Rui Qi, Miguel Alonso

Phase Space Tomography for Measuring Partially Coherent Fields of Light Sources

Rui Qi[1] and Miguel A. Alonso[2,3*]

[1]Department of Physics and Optical Science, The University of North Carolina at Charlotte, NC, 28262, USA

[2]Aix Marseille Univ, CNRS, Centrale Med, Institut Fresnel, Marseille, 13013, France.

[3]The Institute of Optics, University of Rochester, Rochester, NY,14627, USA.

[*]Corresponding author: miguel.alonso@fresnel.fr

We implement experimentally a method for characterizing the two-point coherence properties of fields in two dimensions from measurements of their irradiance at different propagation distances. This method is a form of phase space tomography, based on a definition of the ambiguity function that is appropriate beyond the paraxial regime. In the experiment, a combination of two cylindrical lenses is used to create focused fields that vary slowly in one direction, so they behave approximately like two-dimensional fields. Four types of light sources (an incandescent lamp, a white LED, a green LED, and a green laser) with different coherence properties were measured. The results of the method for nonparaxial fields are compared to those based on the paraxial approximation.

1. INTRODUCTION

It is an honor to be invited to contribute to this Special Issue that celebrates the many contributions of Prof. Anna Consortini both to optical science and its dissemination throughout the world. One of us (MAA) has had the privilege of knowing Prof. Consortini for almost 30 years. During my student years we had a few discussions at a couple of conferences. Immediately following my PhD defense I traveled to Italy, and I visited Prof. Consortini at the University of Florence. She showed me her laboratory and the very interesting work she was doing. One thing that I will always remember is that she was the first person to introduce me to her colleagues as “Dr. Alonso”. Since then, I’ve been extremely lucky to collaborate extensively with Prof. Consortini, not on research (yet) but on optics education aimed especially at young scientists from economically developing countries. At these events, I typically teach theoretical aspects, while she coordinates laboratory sessions to illustrate optical phenomena such as diffraction. An expert in the propagation of light through the atmosphere, Prof. Consortini always stresses the importance of understanding the mathematical foundations of wave propagation and the corresponding statistical

aspects [1, 2]. We therefore thought that it would be appropriate to contribute to this Special Issue a description of the experimental implementation of a method for characterizing partially coherent light through its propagation properties.

Phase space tomography is a technique used in a range of different physical contexts for characterizing partially coherent wave fields in space or time, as well as quantum mixed states [3–9]. Let us focus on the context of spatially partially coherent optical fields, where the spatial coherence of a beam in the frequency domain is characterized by a quantity known as the cross-spectral density [10]. Phase space tomography allows retrieving the cross-spectral density from measurements of the local spectral density (i.e. the irradiance component at the corresponding frequency) at planes corresponding to different propagation distances. Each of these measurements gives access to projections or sections of a phase space representation such as the Wigner function [11, 12] or the ambiguity function [12, 13].

The mathematical framework of phase space tomography was suggested in 1987 by Bertrand and Bertrand [3]. The idea is that different measurements correspond to projections of the Wigner function in different directions in phase space, so that this function can be estimated from a number of such measurements by using the inverse Radon transform [14]. This method was first used to characterize temporal coherence in short pulses [5], as well as the quantum state of a light mode [6]. Its use for the characterization of the spatial coherence of paraxial optical fields was proposed by Nugent [4] and implemented by Raymer's group [7, 8], who also noted that the direct use of phase space tomography is limited to one transverse dimension, and that its extension to two transverse dimensions would require also many measurements with different sets of cylindrical lenses. Cámara *et al.* [15] implemented a method where the cylindrical lenses are replaced with spatial light modulators, allowing a more efficient characterization of the Wigner function and hence the field.

A formally equivalent but mathematically simpler approach to phase space tomography was proposed by Tu and Tamura [16] based on the ambiguity function [13], which is the Fourier transform in both the position and direction variables of the Wigner function. In this approach, one-dimensional (1D) Fourier transforms of the measured irradiances of a two-dimensional (2D) paraxial field at different distances give directly slices of the ambiguity function along radial lines in phase space. The ambiguity function can then be estimated by interpolating from these slices. The spatial coherence of the paraxial field is then found as the Fourier transform of the ambiguity function over the angular separation direction [16]. Whether it is based on the Wigner or ambiguity functions, the standard formalism for phase

tomography is limited to the paraxial domain. A theoretical generalization to the nonparaxial regime was proposed by Cho and Alonso [17], based on a generalized ambiguity function for nonparaxial fields.

The goal of this study is to provide an experimental implementation of phase space tomography for light sources with different coherence levels, and extract their cross-spectral density by employing both the paraxial [16] and nonparaxial [17] approaches, such that their results are compared for real sources whose light is not strictly paraxial. Furthermore, Wigner functions are also calculated to verify the reconstructed ambiguity functions. Section 2 discusses the methods of calculation. Section 3 demonstrates the experimental setups and results. Section 4 discusses the findings of the study. Finally, Section 4 provides some concluding remarks.

2. THEORETICAL BACKGROUND

A. Partially coherent beams in 2D

Consider a stationary partially coherent scalar field with cylindrical symmetry, such that it only depends on a transverse variable x and the propagation direction z. The field is assumed to propagate towards larger values of z but it is not necessarily paraxial. To within second-order coherence theory, this field is described by the cross-spectral density [10], $W(x_1, x_2; z; \omega)$, which describes the statistical correlation of the field at the points (x_1, z) and (x_2, z) at the frequency ω. This function is defined as

$$W(x_1, x_2; z; \omega) = \langle U^*(x_1; z; \omega) U(x_2; z; \omega) \rangle, \tag{1}$$

where the brackets represent a time average, and $U(x_i; z; \omega)$ is the scalar complex field amplitude at position $(x_i; z)$ for frequency ω. When the two points x_1 and x_2 coincide, the cross-spectral density reduces to the spectral density, which is the component of the irradiance at frequency ω measured at the point in question:

$$S(x; z; \omega) = W(x, x; z; \omega) = \langle |U(x; z; \omega)|^2 \rangle. \tag{2}$$

In what follows we drop the dependence in ω for brevity.

B. Phase Space Tomography for Paraxial Fields

The ambiguity function is a phase space distribution proposed within the context of radar that was later introduced for the study of optical fields [13]. For a paraxial partially coherent optical field, it can be defined in terms of the cross-spectral density as

$$\mathcal{A}_{\mathrm{p}}(x', z; p') = \frac{k}{2\pi} \int W\left(x - \frac{x'}{2}, x + \frac{x'}{2}; z\right) \exp(-ikxp')\, dx, \tag{3}$$

where the variables x' and p' can be regarded as separations in the spatial and directional domains, respectively, and $k = \omega/c = 2\pi/\lambda$ is the free space wavenumber, with c being the speed of light and λ the wavelength. The ambiguity function has the property of describing paraxial propagation in terms of a simple rearrangement of its arguments:

$$\mathcal{A}_{\mathrm{p}}(x', z; p') = \mathcal{A}_{\mathrm{p}}(x' - zp', 0; p'). \tag{4}$$

These two equations are the key to Tu and Tamura's phase space tomography approach [16]: by setting $x' = 0$ we see that the Fourier transform of the spectral density at propagation distance z gives the ambiguity function at $z = 0$ (or z_0) at a radial slice with slope $-z$ in the phase space (x', p'), that is

$$\mathcal{A}_{\mathrm{p}}(-zp', 0; p') = \frac{k}{2\pi} \int S(x, z) \exp(-ikxp')\, dx. \tag{5}$$

Figure 1 illustrates the relationship between the spectral density and the ambiguity function. Therefore, if the spectral density is measured at a sufficient number of propagation distances, the ambiguity function is determined at a series of radial slices, from which the remaining values can be estimated through interpolation. The cross-spectral density can then be estimated from the inverse of Eq. (3), namely

$$W\left(x - \frac{x'}{2}, x + \frac{x'}{2}; z\right) = \int \mathcal{A}_{\mathrm{p}}(x', z; p') \exp(-ikxp')\, dp'. \tag{6}$$

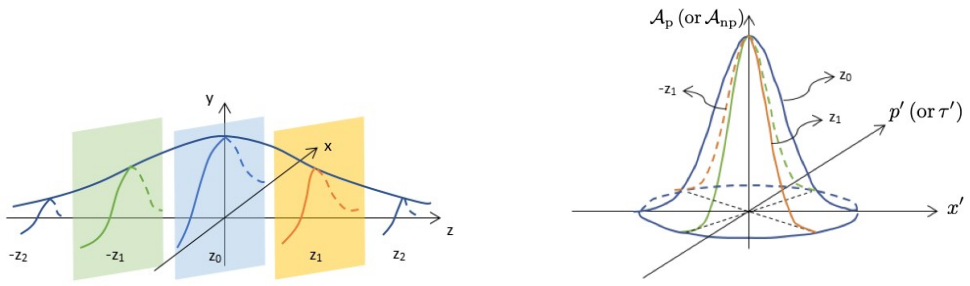

(a) (b)

Fig. 1. Relationship between (a) spectral density and (b) an ambiguity function: the Fourier transform of the cross-sections of constant z of the spectral density correspond to radial slices of the ambiguity function.

C. Phase Space Tomography for Nonparaxial Fields

Note that the approach just described cannot be applied in the nonparaxial regime, since for the ambiguity function defined in Eq. (3), nonparaxial propagation does not simply correspond to a rearrangement of arguments, as in Eq. (4). However, a nonparaxial version of the ambiguity function can be defined in terms of the correlation of the plane-wave components of the field [17]. This nonparaxial generalization does satisfy an argument rearrangement property:

$$\mathcal{A}_{\mathrm{np}}(x', z; \tau') = \mathcal{A}_{\mathrm{np}}(x' - z\tau', 0; \tau'). \tag{7}$$

where the variable τ' corresponds to a difference in the tangents of the angles of propagation of two plane wave components of the field. It is this nonparaxial generalization that is related to the spectral density through a Fourier transform:

$$\mathcal{A}_{\mathrm{np}}(-z\tau', 0; \tau') = \frac{k}{2\pi}\int S(x, z)\exp(-ikx\tau')\,dx. \tag{8}$$

The correlation of plane wave components of field is the inverse Fourier transform of the nonparaxial ambiguity function [17]:

$$\left\langle A^*\left[\theta - \frac{\bar{\alpha}(\tau',\theta)}{2}\right] A\left[\theta + \frac{\bar{\alpha}(\tau',\theta)}{2}\right]\right\rangle = \frac{k}{2\pi}\frac{\sqrt{4\cos^2\theta - \tau'^2}}{2\cos^2\theta}\int \mathcal{A}_{\mathrm{np}}(x', 0; \tau')\exp(-ikx'\tan\theta)\,dx' \tag{9}$$

where θ is the angle between the direction of propagation of plane waves and the z axis, and $\bar{\alpha}(\tau', \theta) = 2\arcsin\frac{\tau'}{2\cos\theta}$ is a function of τ' and θ from a change of variables. The cross-spectral density can then be calculated from the angular spectrum correlation as [17]

$$W(x_1, z; x_2, z) = \iint \langle A^*(\theta_1)A(\theta_2)\rangle \exp\{\mathrm{ik}[\mathrm{x}_2\sin\theta_2 - x_1\sin\theta_1 + z(\cos\theta_2 - \cos\theta_1)]\}\,\mathrm{d}\theta_1\mathrm{d}\theta_2. \tag{10}$$

D. The Wigner Function

The Wigner function is a phase space distribution introduced within the context of quantum physics [11] and then applied (or introduced independently) to a range of other fields, including optics a wave-optical foundation for the heuristic formalism of radiometry [12, 18–20], given that its properties resemble those of the radiance [21, 22].

Let us consider first the paraxial regime. The Wigner function, written here as $B_{\mathrm{p}}(x, z; p)$, is related through Fourier transformation over both x' and p' to the ambiguity function

$$B_{\mathrm{p}}(x, z; p) = \frac{k}{2\pi}\iint \mathcal{A}_{\mathrm{p}}(x', z; p')\exp[ik(xp' - x'p)]\,dx'dp', \tag{11}$$

where x represents a position and p a propagation direction. As mentioned earlier, the Wigner function behaves like a radiance, that is, as a weight for the rays specified by their position (x, z) and direction p. The integral of the Wigner function over all directions (that is, projecting it onto the position axis) gives the spectral density,

$$\int B_{\mathrm{p}}(x, z; p)\ dp = S(x, z). \tag{12}$$

Paraxial propagation corresponds also to an argument rearrangement for the Wigner function according to the rectilinear propagation of rays:

$$B_{\mathrm{p}}(x, z; p) = B_{\mathrm{p}}(x - zp, 0; p). \tag{13}$$

These expressions allow calculating the spectral density from the knowledge of the Wigner function at any plane $z = z_0$.

While the description above is valid for paraxial fields, a nonparaxial version of the Wigner function, denoted here as $B_{\mathrm{np}}(x, z; \tau)$, has been defined [23] that is related to the nonparaxial ambiguity function through a relation identical to Eq. (11) with $\mathcal{A}_{\mathrm{p}}$ replaced with $\mathcal{A}_{\mathrm{np}}$. This nonparaxial Wigner function satisfies the analogue of the projection property in Eq. (12) and of the rectilinear propagation property in Eq. (13), both with p replaced by τ.

3. EXPERIMENT RESULTS

A. Experiment Setups

In the experiment, a green LED ($\lambda_p = 555nm$, $U = 2.8V$, $I = 20mA$), a white LED ($V = 3.0V$, $I = 20mA$), an incandescent lamp ($U = 1V$, $I = 260mA$), and a laser ($\lambda_p = 532nm$, $P = 6mW$), are selected as test light sources. Figure 2a shows the experiment setup for measuring the first three (partially coherent) sources. A horizontal slit (HS) is placed in front of the light source (LS) to confine the field into a general line shape. An iris is used to block the stray light not falling onto the following lenses. The combination of a horizontal cylindrical lens, CL_1 ($f = 150mm$), and a vertical cylindrical lens, CL_2 ($f = 100mm$), creates the 2D light fields. A 2D charge-coupled device (CCD) array (Imagingsource DMK-31BF03, 1024X768) moves near the focus distance z_0 along the z axis to detect the spectral density. The entire line-shaped field is captured by the CCD array, so there is no need to move the CCD along the x direction. Figure 2b illustrates the experiment setup for measuring a coherent source (a green laser). A neutral density filter (ND) is inserted in front of the laser to minimize the CCD saturation. Additionally, a beam expander (BE), which consists of two collimating lenses and a pinhole, is placed after the ND to expand the laser beam.

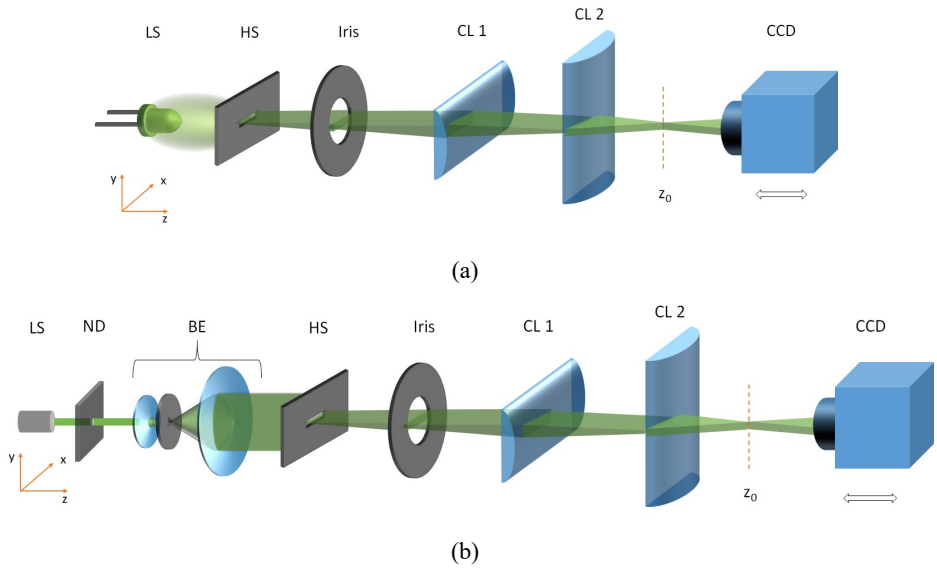

Fig. 2. Experimental setups for measuring optical fields of (a) partially coherent and (b) laser sources.

B. Irradiance Distribution

Each light source is measured at a number of distances N before and after the focusing position z_0. In the experiment, $N_{\text{incandescent}} = 63$, $N_{\text{whiteLED}} = 69$, $N_{\text{greenLED}} = 61$, and $N_{\text{laser}} = 57$. The increments for the displacements are of $d = 200\mu m$ near z_0 and $d = 500\mu m$ into the far field. Table 1 summarizes the measurement distance ranges and the estimated nonparaxial angles.

Table 1. Measurement Distance Ranges and Nonparaxial Angles of Each Light Source

Parameters	Incandescent	White LED	Green LED	Laser
Distance z (mm)	[-15.8, 9.8]	[-17.8, 10.8]	[-12.8,11.5]	[-14.8,7.5]
Half beam angle (°)	9	7	11	9

Figure 3 shows the cross-sections of the irradiance distribution of light sources near z_0 captured by a CCD. Figure 4 shows top views of irradiance distributions in the x and the z directions. The irradiance values of each measurement are summed over the narrow width along the y axis to obtain a 1D distribution along the x axis. Subsequently, a stacking of the 1D distributions gives the 2D distribution.

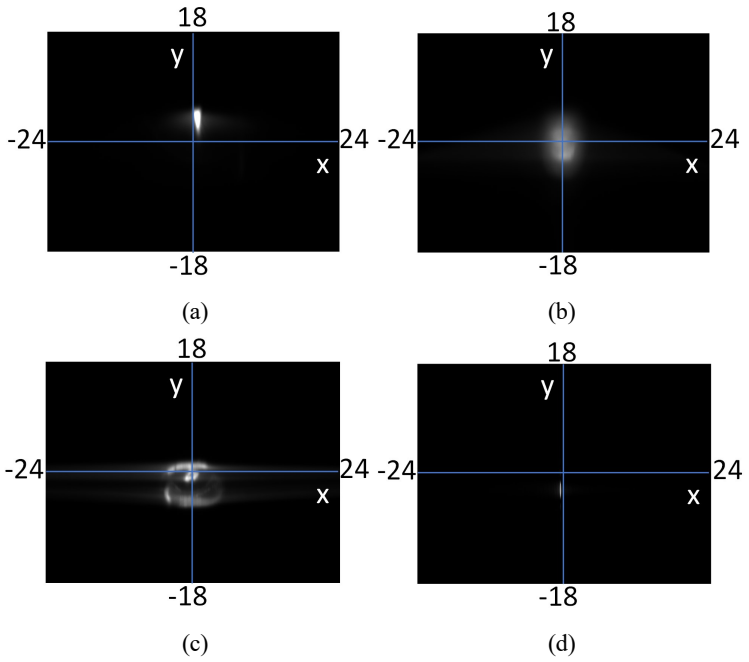

Fig. 3. Cross-sections of irradiance distribution at the plane $z = z_0$ measured on a CCD in unit of mm of (a) an incandescent lamp, (b) a white LED, (c) a green LED, and (d) a laser.

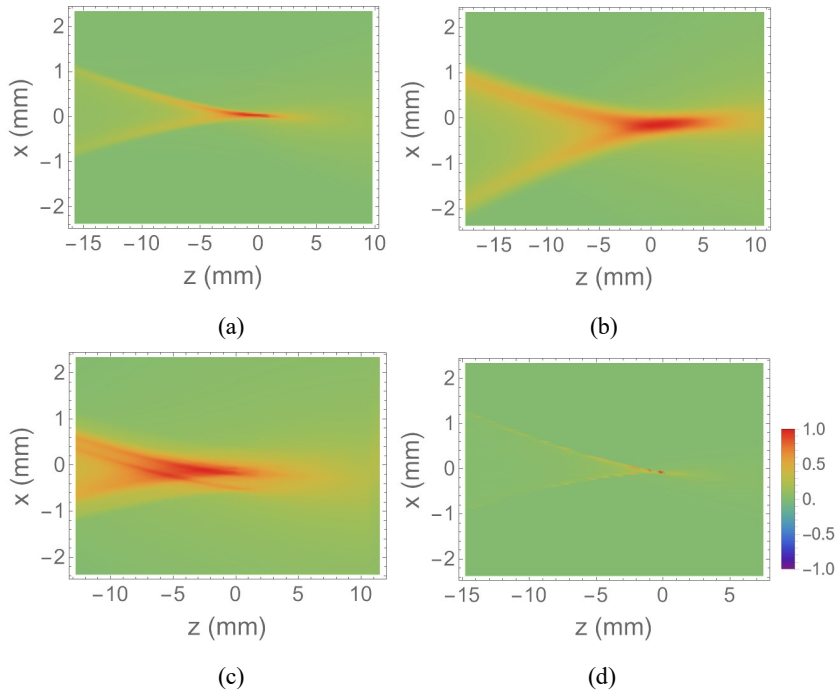

Fig. 4. Top views of the irradiance distribution for (a) an incandescent lamp, (b) a white LED, (c) a green LED, and (d) a laser.

The procedure that follows for calculating the ambiguity function and from it the cross-spectral density requires specifying the wavelength of the light. For the green LED and the laser, the quasi-monochromatic

approximation is valid, so we can simply use their central wavelengths (555*nm* and 532*nm*, respectively). The white LED and the incandescent lamp, on the other hand, have broader spectra. To process the data, we make a gray world approximation in which we assume that the spectral density distribution is approximately the same for all frequency components. The calculations then focus on the retrieval of the cross-spectral density for $\lambda = 500nm$.

C. Reconstruction of the Ambiguity Function

To calculate the ambiguity function, a discrete Fourier transform (DFT) is taken on each 1D irradiance distribution at different distance. Then, the coordinates of p' (or τ') and x' of the discrete ambiguity function values are identified. Finally, a combination of the DFT radial slices leads to the ambiguity functions. To avoid an oversampling at $x' = 0$, only the DFT value at $x' = 0$ measured at z_0 is taken. Figure 5 illustrates the top views of the real part of the reconstructed ambiguity functions at z_0. Notice that up to now the reconstruction is independent of whether the paraxial or nonparaxial approaches are being used.

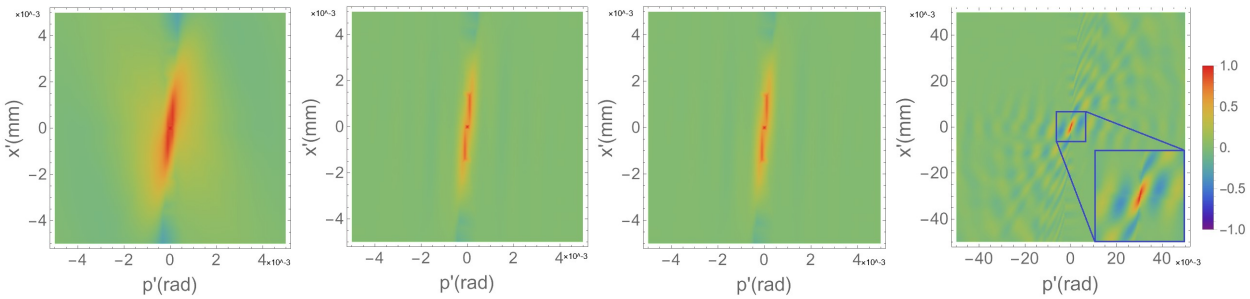

Fig. 5. Real part of the ambiguity functions at z_0 reconstructed from (a) an incandescent lamp, (b) a white LED, (c) a green LED, and (d) a laser.

D. Cross-Spectral Density

If we assume we are in the paraxial regime, the cross-spectral density at $z = z_0$ is calculated from the reconstructed ambiguity function by taking the Fourier transform over p'. Figure 6 illustrates the amplitude and phase of the results. The horizontal axis represents the x coordinate in *mm* and the vertical axis represents the x' coordinate in *mm*.

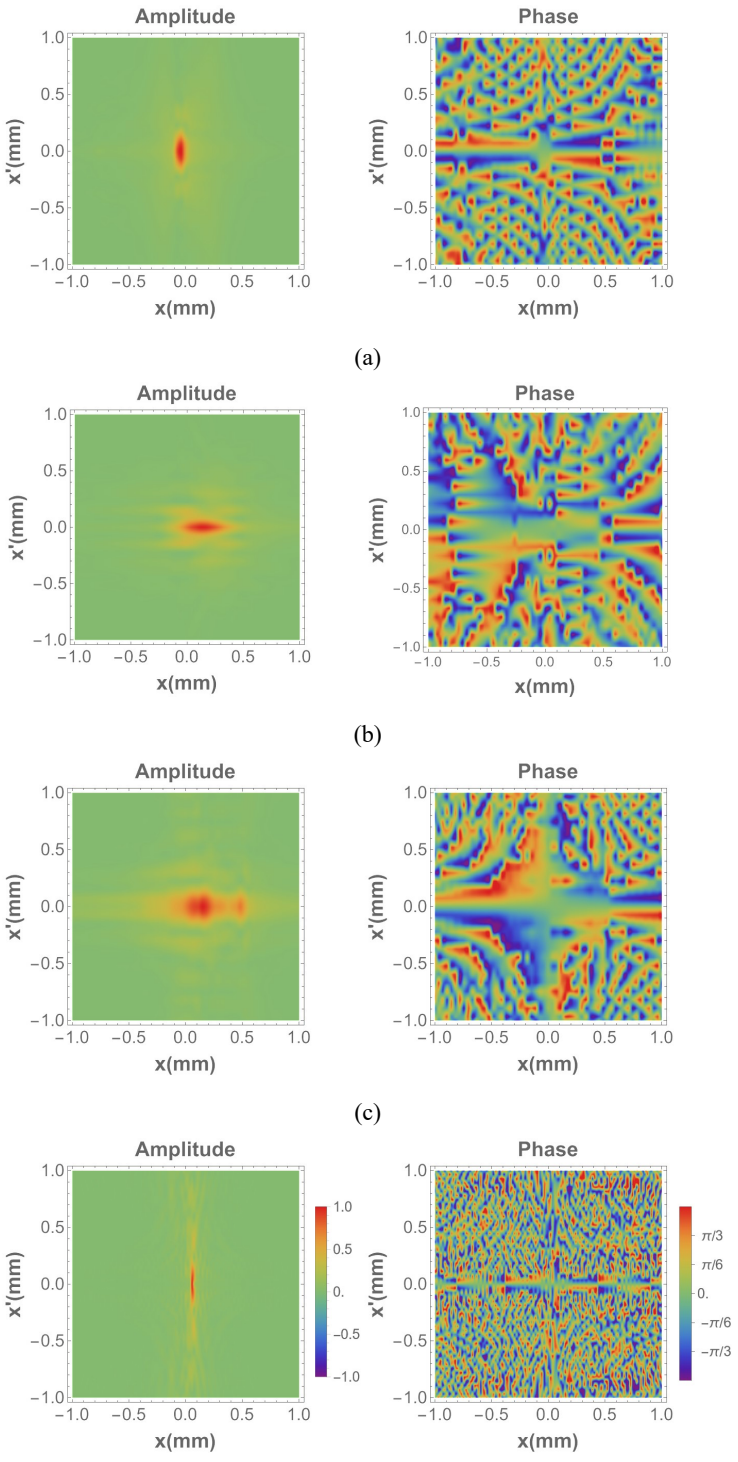

Fig. 6. Amplitude and phase of the cross-spectral density function at z_0 based on a method for a paraxial field reconstructed from (a) an incandescent, (b) a white LED, (c) a green LED, and (d) a laser. Here, x is the centroid of the two points and x' their separation.

To extract the cross-spectral density based on the method for a nonparaxial field, the angular spectrum correlation is first calculated by taking one-dimensional Fourier transform over an ambiguity function and then applying an envelope over the Fourier transformed ambiguity function. Figure 7 illustrates the amplitudes of angular spectrum correlations. One axis represents the $\bar{\alpha}$ coordinate and the other axis represents the θ coordinate.

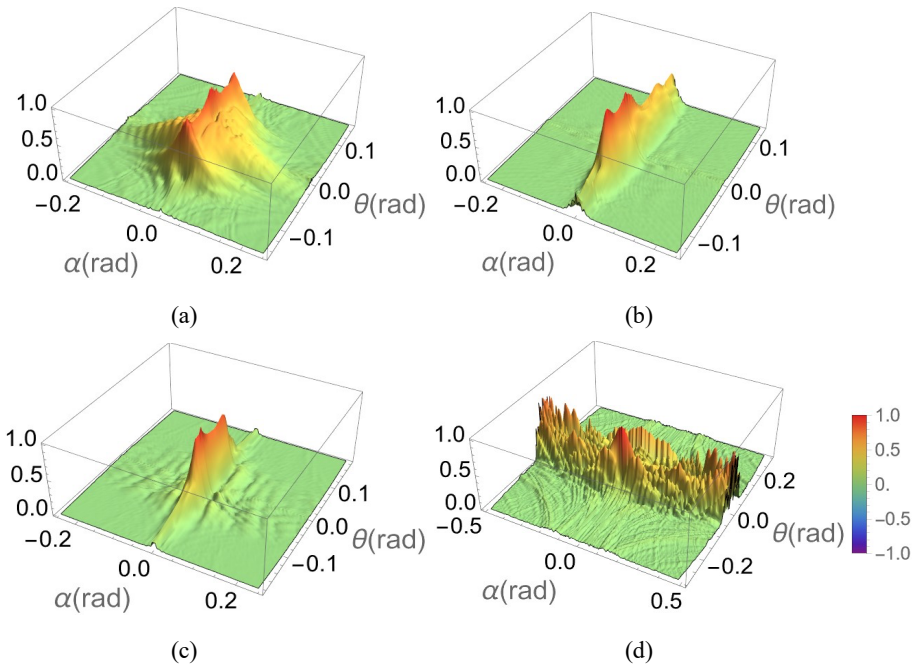

Fig. 7. Amplitude of the angular spectrum correlation reconstructed from (a) an incandescent, (b) a white LED, (c) a green LED, and (d) a laser.

The nonparaxial cross-spectral density is then calculated from angular spectrum correlations and is compared with those calculated by using the paraxial method. Table 2 lists amplitude errors of normalized cross-spectral density of each light source based on the paraxial method. The cross-spectral densities calculated by using the two methods are normalized, and then the difference is estimated by $\Delta CSD_{peak} = |CSD_{peak-p} - CSD_{peak-np}|$. The shapes of the cross-spectral densities resulting from both methods look similar, which might due to the relatively small half beam angles created in the experiment. Figure 8 illustrates the amplitude difference of the cross-spectral density by using the paraxial and nonparaxial methods.

Table 2. Amplitude Errors of Normalized Cross-spectral Density of Light Sources based on the Paraxial Method

Parameters	Incandescent	White LED	Green LED	Laser
Error	0.01	0.006	0.015	0.08

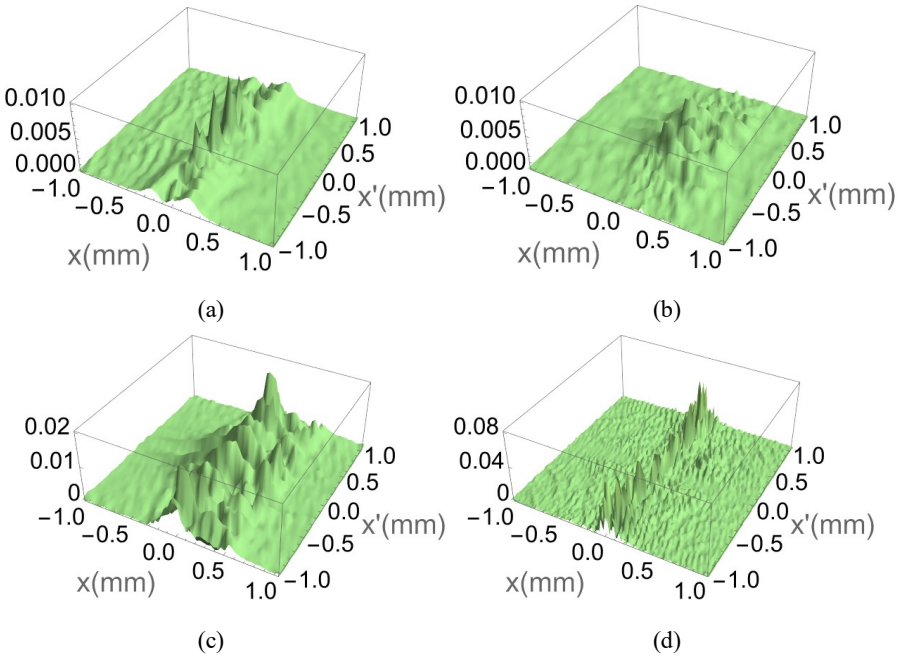

Fig. 8. Amplitude of the cross-spectral density by using the paraxial method, reconstructed from (a) an incandescent, (b) a white LED, (c) a green LED, and (d) a laser.

Note that there can be some experimental sources residual error. One of them is the possible misalignment of the two cylindrical lenses, which would cause asymmetrical beams down the optical path. Another is saturation of the CCD occurring near the focal point of the two cylindrical lenses. Finally, some light leaks outside the CCD toward the far end of the measurement range for the incandescent lamp, the white LED, and especially for the green LED.

E. Result Verification

Wigner functions are calculated by a 2D DFT on the ambiguity functions. Figure 9 illustrates the top views of reconstructed Wigner function at z_0. The horizontal axis represents the x coordinate in *mm* and the vertical axis represents slope (which is dimensionless).

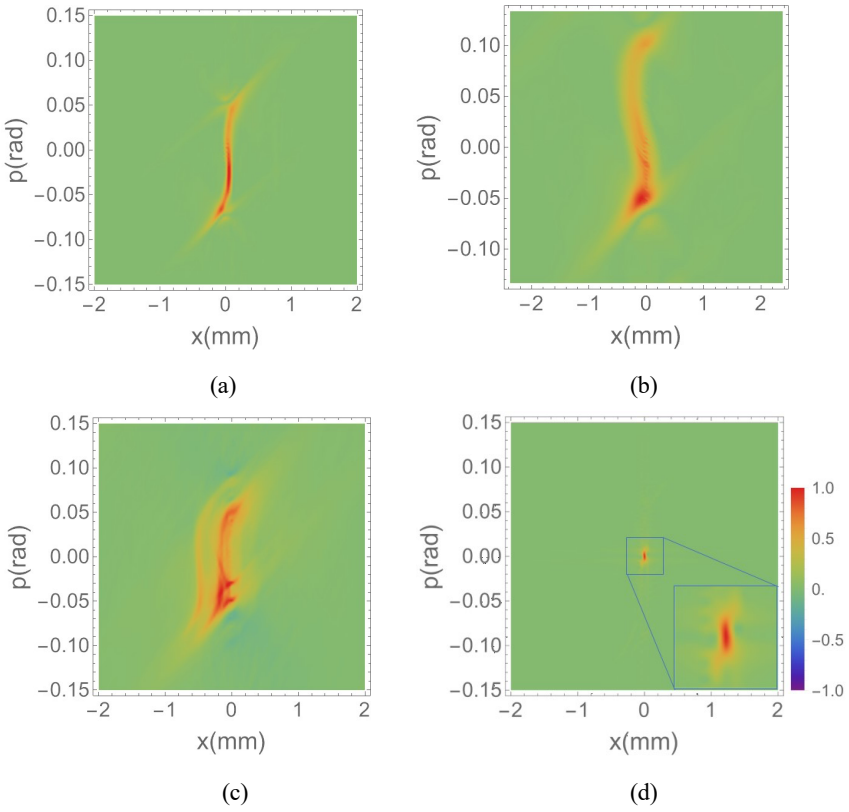

Fig. 9. Wigner function at z_0 reconstructed from (a) an incandescent, (b) a white LED, (c) a green LED, and (d) a laser.

As discussed in Section 2, the projection of a Wigner function on the x axis gives the irradiance distribution of a linear field. Here, projections of the Wigner function at different distances z are calculated by shearing the Wigner function at z_0 following Eq. (12). Then, the field is recovered for verifying the ambiguity functions. The measured fields and the reconstructed fields from Wigner functions are firstly normalized, and then one is subtracted from the other. Figure 10 shows the estimated errors. The reconstructed fields, except that of the laser, have an error within 15%. The reconstructed laser field has more significant errors due to its spiky and noisy shape.

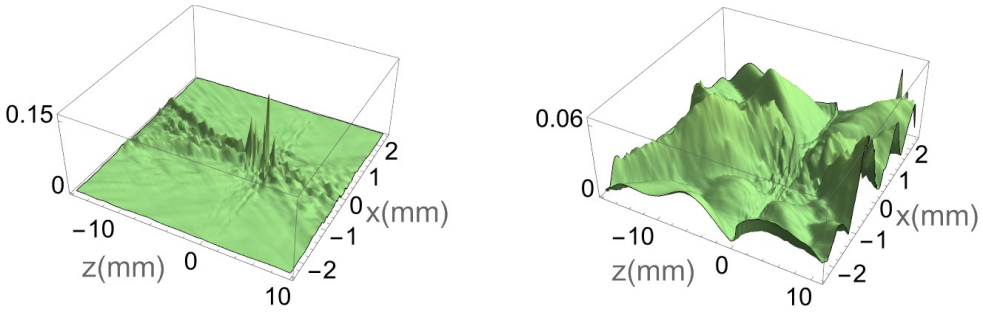

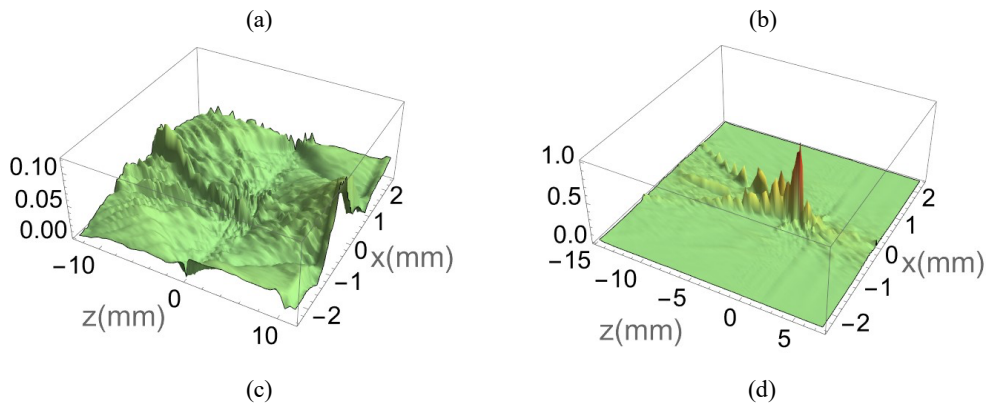

Fig. 10. Isometric views of difference between measured field distributions and those recovered from Wigner functions of (a) an incandescent, (b) a white LED, (c) a green LED, and (d) a laser.

4. DISCUSSION AND CONCLUSION

This study provides a review of the technique of phase space tomography for the retrieval of the cross-spectral density for fields with cylindrical symmetry, and reports on the first experimental implementation of one such technique valid in the nonparaxial regime. The results of this method are compared with those based on the paraxial approximation. Both methods rely on taking the inverse Fourier transform of the measured irradiance distributions over a range of propagation distances. In the experiment, four types of light sources with narrow and broad spectrum are measured.

The resulting cross-spectral density estimates for both methods are fairly similar, probably because of the relatively narrow half-angles of the beams. The errors are up to 0.015% for the partially coherent sources with a 11º half-angle, and 0.08% for the laser source with a 9º half-angle. These errors are below the level of error introduced by the numerical approximations coming from the sampling and interpolation, as well as from the experimental limitations mentioned earlier. It would be interesting to compare the two approaches for a more strongly focused partially coherent field.

The advantages of the phase space tomography technique are that no interferometric setup is required; it suffices to measure the irradiance at different propagation distances, and the results are valid for measuring both paraxial and nonparaxial fields of any level of spatial coherence. The drawback is that the approach is limited to fields with cylindrical symmetry, that is, which are (at least approximately) independent of y.

The experiment results demonstrate the spherical aberration of the optical path in both the field distribution plots and the reconstructed Wigner functions. The irradiance distributions show that the spherical aberration causes

the optical beams at the edge of the field to converge faster than those near the center. This aberration is easily visualized in the plots of the Wigner functions, which present an s-shaped distribution.

The differences in coherence level of the four types of light sources are clearly demonstrated by the plots of ambiguity functions. In particular, the plots for the laser source demonstrate strong oscillations in phase space, while these oscillations are washed out for partially coherent light sources. The results of ambiguity and Wigner functions are consistent with the theoretical prediction [17].

5. BACKMATTER

Acknowledgments.

The authors thank Greg Gbur for support and discussions, and John Marciante for guidance with the experimental implementation. MAA wishes to thank also the Abdus Salam International Centre of Theoretical Physics in Trieste, Italy, where between 2006 and 2020 he worked with Prof. Consortini and other colleagues including Imrana Ashraf, Miltcho Danailov and Humberto Cabrera on the organization and teaching of the Preliminary School to the Winter College in Optics. Particular thanks go to the late Gallieno Denardo and to Joe Niemela, who led the organization of these events. Finally, we thank the organizers of this Special Issue.

Disclosures.

The authors declare no conflicts of interest.

Data Availability Statement.

Data underlying the results presented in this paper are not publicly available at this time but may be obtained from the authors upon reasonable request.

REFERENCES

1. A. Consortini, “How much mathematics should optics students know?” in *Proc. SPIE,* , vol. 1603 (1991).
2. A. Consortini, “Should optics students know statistics?” in *Education and Training in Optics and Photonics,* (Optica Publishing Group, 1999), p. OS47.
3. J. Bertrand and P. Bertrand, Found. Phys. **17**, 397 (1987).
4. K. A. Nugent, Phys. Rev. Lett. **68**, 2261 (1992).
5. M. Beck, M. Raymer, I. Walmsley, and V. Wong, Opt. Lett. **18**, 2041 (1993).
6. D. Smithey, M. Beck, M. G. Raymer, and A. Faridani, Phys. Rev. Lett. **70**, 1244 (1993).
7. M. Raymer, M. Beck, and D. McAlister, Phys. Rev. Lett. **72**, 1137 (1994).
8. D. McAlister, M. Beck, L. Clarke, A. Mayer, and M. Raymer, Opt. Lett. **20**, 1181 (1995).
9. U. Leonhardt, *Measuring the quantum state of light*, vol. 22 (Cambridge university press, 1997).
10. M. Born and E. Wolf, *Principles of optics: electromagnetic theory of propagation, interference and diffraction of light* (Elsevier, 2013).
11. E. Wigner, Phys. review **40**, 749 (1932).

12. M. A.Alonso, Adv. Opt. Photonics **3**, 272 (2011).
13. A. Papoulis, J. Opt. Soc. Am. **64**, 779 (1974).
14. A. W. Lohmann, J. Opt. Soc. Am. A **10**, 2181 (1993).
15. A. Cámara, T. Alieva, J. A. Rodrigo, and M. L. Calvo, J. Opt. Soc. Am. A **26**, 1301 (2009).
16. J. Tu and S. Tamura, J. Opt. Soc. Am. A **15**, 202 (1998).
17. S. Cho and M. A. Alonso, J. Opt. Soc. Am. A **28**, 897 (2011).
18. L. DOLIN, 1964. pp. 244–249 (1964).
19. A. Walther, JOSA **58**, 1256 (1968).
20. M. J. Bastiaans, Opt. communications **25**, 26 (1978).
21. E. Wolf, JOSA **68**, 6 (1978).
22. A. T. Friberg, Appl. optical coherence **194**, 55 (1979).
23. K. B. Wolf, M. A. Alonso, and G. W. Forbes, JOSA A **16**, 2476 (1999).

FULL REFERENCES

1. A. Consortini, "How much mathematics should optics students know?" in *Proc. SPIE,* vol. 1603 (1991).
2. A. Consortini, "Should optics students know statistics?" in *Education and Training in Optics and Photonics,* (Optica Publishing Group, 1999), p. OS47.
3. J. Bertrand and P. Bertrand, "A tomographic approach to Wigner's function," Found. Phys. **17**, 397–405 (1987).
4. K. A. Nugent, "Wave field determination using three-dimensional intensity information," Phys. Rev. Lett. **68**, 2261 (1992).
5. M. Beck, M. Raymer, I. Walmsley, and V. Wong, "Chronocyclic tomography for measuring the amplitude and phase structure of optical pulses," Opt. Lett. **18**, 2041–2043 (1993).
6. D. Smithey, M. Beck, M. G. Raymer, and A. Faridani, "Measurement of the Wigner distribution and the density matrix of a light mode using optical homodyne tomography: Application to squeezed states and the vacuum," Phys. Rev. Lett. **70**, 1244 (1993).
7. M. Raymer, M. Beck, and D. McAlister, "Complex wave-field reconstruction using phase-space tomography," Phys. Rev. Lett. **72**, 1137 (1994).
8. D. McAlister, M. Beck, L. Clarke, A. Mayer, and M. Raymer, "Optical phase retrieval by phase-space tomography and fractional-order Fourier transforms," Opt. Lett. **20**, 1181–1183 (1995).
9. U. Leonhardt, *Measuring the quantum state of light*, vol. 22 (Cambridge university press, 1997).
10. M. Born and E. Wolf, *Principles of optics: electromagnetic theory of propagation, interference and diffraction of light* (Elsevier, 2013).
11. E. Wigner, "On the quantum correction for thermodynamic equilibrium," Phys. review **40**, 749 (1932).
12. M. A.Alonso, "Wigner functions in optics: describing beams as ray bundles and pulses as particle ensembles," Adv. Opt. Photonics **3**, 272–365 (2011).
13. A. Papoulis, "Ambiguity function in fourier optics," J. Opt. Soc. Am. **64**, 779–788 (1974).
14. A. W. Lohmann, "Image rotation, Wigner rotation, and the fractional fourier transform," J. Opt. Soc. Am. A **10**, 2181–2186 (1993).
15. A. Cámara, T. Alieva, J. A. Rodrigo, and M. L. Calvo, "Phase space tomography reconstruction of the Wigner distribution for optical beams separable in cartesian coordinates," J. Opt. Soc. Am. A **26**, 1301–1306 (2009).
16. J. Tu and S. Tamura, "Analytic relation for recovering the mutual intensity by means of intensity information," J. Opt. Soc. Am. A **15**, 202–206 (1998).
17. S. Cho and M. A. Alonso, "Ambiguity function and phase-space tomography for nonparaxial fields," J. Opt. Soc. Am. A **28**, 897–902 (2011).
18. L. DOLIN, "Beam description of weakly-inhomogeneous wave fields(beam description of weakly inhomogeneous wave fields)," 1964. pp. 244–249 (1964).
19. A. Walther, "Radiometry and coherence," JOSA **58**, 1256–1259 (1968).
20. M. J. Bastiaans, "The wigner distribution function applied to optical signals and systems," Opt. communications **25**, 26–30 (1978).
21. E. Wolf, "Coherence and radiometry," JOSA **68**, 6–17 (1978).
22. A. T. Friberg, "Effects of coherence in radiometry," Appl. optical coherence **194**, 55–70 (1979).
23. K. B. Wolf, M. A. Alonso, and G. W. Forbes, "Wigner functions for helmholtz wave fields," JOSA A **16**, 2476–2487 (1999).